

Microconcentrators to recover fill-factor in image photodetectors with pixel on-board processing circuits

Silvano Donati, Giuseppe Martini, Michele Norgia

Università di Pavia, Dipartimento di Elettronica, Via Ferrata 1, 27100, Pavia, Italy
silvano.donati@unipv.it

Abstract: We propose an array of non-imaging micro-concentrators as a mean to recover the loss of sensitivity due to area fill-factor. This is particularly important for those image photo detectors in which complex circuit functions are required and a substantial fraction of the pixel area is consumed, like e.g., 3D camera, SPAD arrays, fluorescence analyzers, etc., but also in CMOS sensors. So far, the low fill-factor was an unacceptable loss of sensitivity precluding from the development of such devices, whereas by using a concentrator array a recovery is possible, up to the inverse square of numerical aperture of the objective lens. By ray tracing, we calculate the concentration factors of several geometries of non-imaging concentrator, i.e., truncated cone, parabolic and compound parabolic, both reflective and refractive. The feasibility of a sizeable recovery of fill-factor (up to 50) is demonstrated.

©2007 Optical Society of America

OCIS codes: (220.1770) Concentrators; (230.5160) Photodetectors; (110.280) Image Enhancement

References

- 1 S. Donati: "Photodetectors," Prentice Hall, Upper Saddle River (NJ) 1999, Appendix A2.
- 2 W.T. Welford, R. Winston: "The Optics of Nonimaging Concentrators," Academic Press, New York, 1978.
- 3 W.T. Welford, J.Minano, P.Benitez: "Nonimaging Optics," Academic Press, New York 2005.
- 4 F. Nakamaru, Y. Matsumoto, A. Nakazano: "Novel high efficiency concentrator for optical communications," IEEE Photonic Techn. Lett., **14** (2002), pp.953-956. (1978).
- 5 P. Benitez, J.C.Minano: "Ultrahigh-numerical-aperture imaging concentrator," J. Opt. Soc Am. **14** (1997), pp.1988-1997.
- 6 J.C. Minano, P.Benitez, and J.C.Gonzalez: "RX, a nonimaging concentrator," Appl. Opt. **34** (1995), pp.2226-2235.
- 7 J. O'Gallagher, R.Winston, W.A.Welford: "Axially symmetric nonimaging flux concentrator with maximum theoretical concentration ratio," J. Opt. Soc Am. **4** (1987), pp.66-68.
- 8 C. Niclass, A. Rochas, P.- A Besse, E.Charbon: "Toward a 3-D camera based on single photon avalanche diode," IEEE J. Sel. Topics in Quant. Electr. **10** (2004), pp.796 – 802.
- 9 S.-I. Chang, J.-B. Yoon, H. Kim, B.-K. Lee, D.H.Shin: "Microlens array diffuser for a light-emitting diode backlight system," Opt. Lett. **31** (2006), pp.3016-3018.

1. Introduction

In image photodetectors, it is very unusual to think of processing the detected current of each pixel by means of on-board circuits allocated around the sensitive area, because even a simple circuit, integrated around the detector, would probably occupy an area comparable or much larger than the detector area and, consequently, spoil the effective sensitivity of the detector. Respect to the normal spectral sensitivity σ (A/W), when the detector has a partial filling η of pixel area, its spectral sensitivity is decreased to $\sigma\eta$, where $\eta=A_d/A_p$ is the (area) fill factor

given by the ratio of detector area A_d to pixel area A_p . Of course, when η is small (e.g. 0.01), the intended application may become impracticable.

In this paper we propose the recovery of the fill factor in an image photodetector by means of an array of individual micro-optical concentrators. Each concentrator collects light from the objective lens in the focal plane and directs it to the sensitive area of the pixel in the detector plane.

Of course, by virtue of the acceptance $\mathfrak{A}=A\Omega$ conservation [1], if power collected on a large pixel area A_p – the collecting area of the concentrator – is to be concentrated on small detector area A_d – the output area of the concentrator – the decrease in area shall be balanced by an equal increase of solid angle Ω , from input to output, of the concentrator.

The solid angle can be written as $\Omega=\pi NA^2$, where $NA= \sin\alpha$ is the (geometrical) numerical aperture of the bundle of rays associated to the emitting or receiving area A , and α is the linear angle of the cone of the aperture. Thus, to obtain a high concentration ratio A_p/A_d we shall sacrifice somehow the numerical aperture NA_L^2 of the objective lens used to direct light onto the photodetector.

Using a low NA_L is sometimes dictated by system requirements – like that of ensuring a reasonable depth of focus, so the concentration corresponding to an $F\#=5.6$ to 11 objective lens, for instance, is given by $NA_L^{-2}=(2 F\#)^2= 125$ to 480, very respectable figures indeed for the concentration theoretically achievable.

The paper is organized as follows: in the next Section we derive the basic relations about concentration, then describe the ray tracing routine we have developed to compute efficiency and concentration of several concentrator geometries, along with the results of the simulations. Finally, we derive some conclusions.

About novelty of the proposed approach, optical concentrators for use with solar cells have been known since a long time [2], and have been fabricated and used with the size of the solar cell – namely centimeters. On the other hand, the possibility of using arrays of sub millimeter-size concentrators to recover an area fill-factor due to on-board circuits in arrays of photodetectors is new, at our best knowledge. Until now, only small single lenses placed in front of a chip have been used to increase the apparent area of the photodetector, but without exploiting the possibility of using the freed space for allocating on-board processing circuits.

This paper presents the results of theoretical evaluations of concentrator geometries only, and will not specifically deal with fabrication. The aim is to support the technical feasibility of the concept of fill-factor recovery, opening the way to a new design concept about on-board processing of signals supplied by a small-area photodetector.

2. Analysis

Let us consider the concentrator as an optical system collecting rays within an aperture with surface of area A_i and solid angle Ω_i , and supplying them at the output on an aperture of area A_o and solid angle Ω_o (Fig. 1). Let the photodetector entrance plane coincide with the output plane of the concentrator and let n_i, n_o be the index of refraction at the input output planes.

Now, we can write the actual power collected by the detector as:

$$P_o = E_o A_o \quad (1)$$

where E_o is the output irradiance. Introducing the concentration factor C as the ratio of output to input irradiances:

$$C = E_o / E_i \quad (2)$$

and substituting in (1), we see that the collected power

$$P_o = C E_i A_o \quad (3)$$

is increased of a factor C respect to the placement of the detector at the input plane.

Of course, power P_o supplied at the output of the concentrator cannot be larger than the input

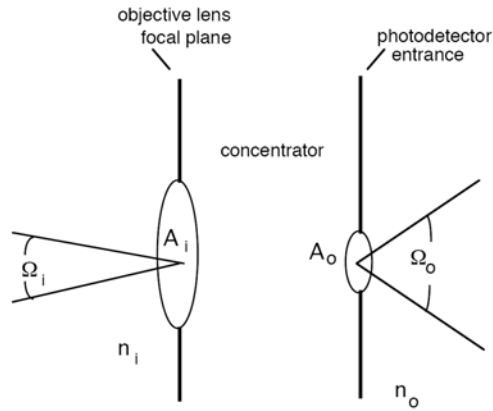


Fig. 1. Light from the objective lens reaches the entrance aperture (of area A_i) under a solid angle Ω_i and the concentrator collects it in a smaller aperture of area A_o within the solid angle Ω_o .

power $P_i = E_i A_i$, and thus we have a first limit to the concentration factor C , set by the ratio of input to output areas:

$$C \leq A_i / A_o \quad (4)$$

Second, let us recall a principle of radiometry [1], that acceptance $n^2 A \Omega$ is an invariant and write:

$$n_i^2 A_i \Omega_i = n_o^2 A_o \Omega_o \quad (5)$$

Assuming $n_i = 1$ and substituting in (4), we get the second limit to the concentration factor C , set by the ratio of input to output solid angles:

$$C \leq n_o^2 \Omega_o / \Omega_i \quad (6)$$

or also, expressing (6) in terms of numerical apertures, being $\Omega_{i,o} = \pi \sin^2 \alpha_{i,o} = NA_{i,o}^2$, we get:

$$C \leq (n_o NA_o / NA_i)^2 \quad (7)$$

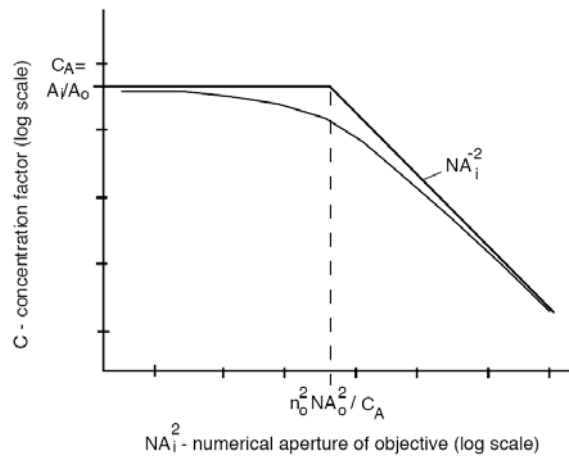


Fig. 2. Dependence of the concentration factor C as a function of numerical aperture NA_i^2 of the objective lens. Horizontal asymptote is set by the area ratio, whereas the roll off as NA_i^2 is due to solid angles ratio. Filling the concentrator with index of refraction n_o moves the break point by a factor n_o^2 to the right. The curve is representative of a real concentrator.

Eqs.(4) and (7) define two asymptotic behavior of the concentration factor versus numerical aperture NA_i of the objective lens, as depicted in Fig.2. At small NA_i , concentration C is a constant and is limited by the area ratio at value $C_A = A_i / A_o$, whereas for large values of NA_i it rolls off as NA_i^{-2} . The value of input numerical aperture at which the roll-off starts is:

$$NA_{iA}^2 = n_o^2 NA_o^2 / C_A \quad (8)$$

From Eq.8 (and Fig.2) we can see that the performance of the concentrator is worsened by a sub-unitary $NA_o < 1$ output numerical aperture, whereas is improved by working in ‘immersion’ conditions, that is with an index of refraction $n_o > 1$ for the medium in which the output is immersed.

This circumstance favors non-imaging concentrators [2,3] in which NA_o approaches unity, respect to lens-based concentrators in which NA_o is the lens numerical aperture, rarely in excess of, say, 0.2 for a single element lens. [However, if the lens material fills all the space available down to detector, a recovery by a factor n_o is achieved].

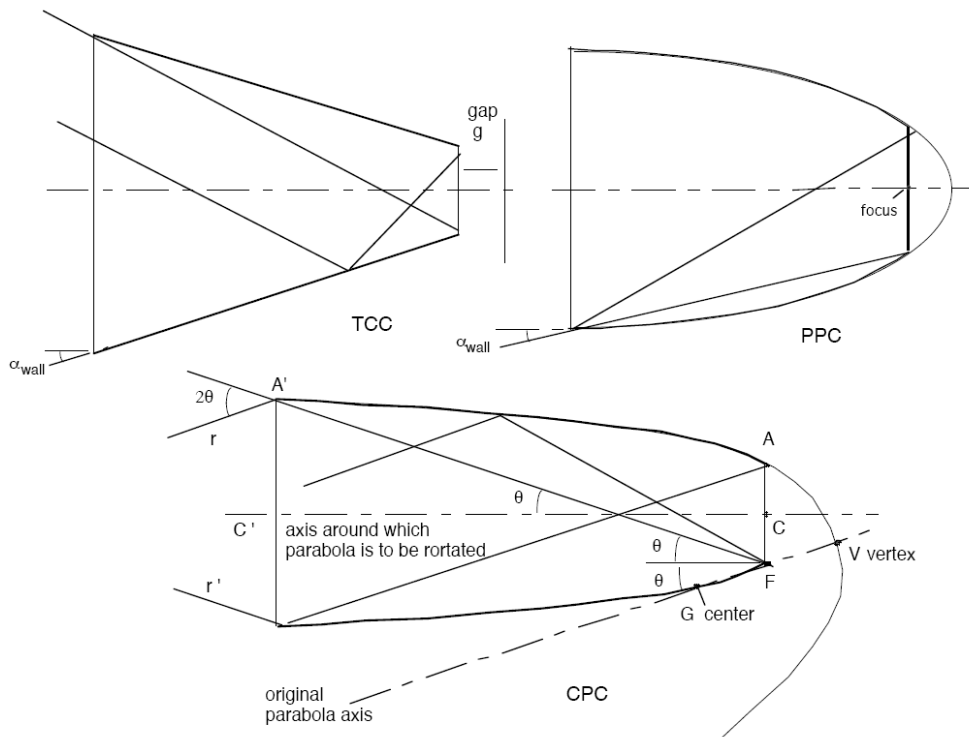


Fig. 3. Geometries of non-imaging concentrators: TCC (truncated-cone concentrator), PPC (plain paraboloid concentrator) and CPC (compound parabolic concentrator)

Also, at equal size and geometry and gap $g=0$, refractive concentrators filled with a material with index of refraction n_o have a better performance than reflective one (in which $n_o=1$ and walls are reflective).

In the following, we present the calculation of concentration factor for three types of rotational geometry: truncated-cone (or TCC), plain paraboloid (PPC) and compound parabolic (CPC) concentrators (see Fig.3) [2,3].

For all these geometries, we have evaluated the concentration factor of the structure in both reflective and refractive cases, that is, either when the concentrator is an empty space structure with ideally reflecting walls, or when structure is filled with a material (n_0) and reflection is because of total reflection at the wall discontinuity.

3. Calculation

A ray-tracing routine has been written to calculate the trajectory of rays entering the input pupil, whether they exit from the output pupil or are lost because reflected back or refracted out of the walls (for refractive types). Rays are assumed to fill uniformly, in space and angle, the input pupil and thus, as shown in Fig.4, we divide the input surface in elemental areas of equal dS , and the input solid angle in elemental angles of equal $d\Omega$. Thus we get four variables (fig.4): ρ , θ , α , and ψ , ranging from: 0 to $D/2$, 0 to 2π , 0 to $\arcsin(NA_i)$ and 0 to 2π , respectively. Now, if we allow a reasonable number of steps to keep the discretization error low, e.g., 20-30 steps to each variable, we get a big number $(20-30)^4$ of rays trajectories that are required to perform the calculation. Fortunately, because of the radial symmetry, just one values of θ is necessary for each ρ , because rays with the same ρ and different θ end in the same way, either collected or rejected. Then, we build a variable N , in which we sum the weight $2\pi\rho$ of the individual ray in the elemental ρ , $\rho+d\rho$ interval (if collected) and 0 (if not collected). Also, we compute the total number of rays N_{TOT} summing all the weights. At the end of calculation, the ratio $N/N_{TOT}=\eta$ is the efficiency of collection of the concentrator, whereas $\eta A_o/A_i=C$ is the concentration factor. Note that elimination of one variable reduces the number of rays to $(20-30)^3$. Another symmetry used to halve the dimensionality is that of ψ , yielding the same result when ranging from $-\pi/2$ to $\pi/2$ and from $\pi/2$ to $3\pi/2$. In total, we need $1/2 (20-30)^3$ rays, now resulting in a manageable computing time (typically, a few second per run on a 2-GHz clock PC).

Rays are then traced and η and C calculated for several lengths L (re-using results of L to calculate $L+\Delta L$ in the TCC) of the concentrator, and for some values of interest of the gap g between output plane and detector surface.

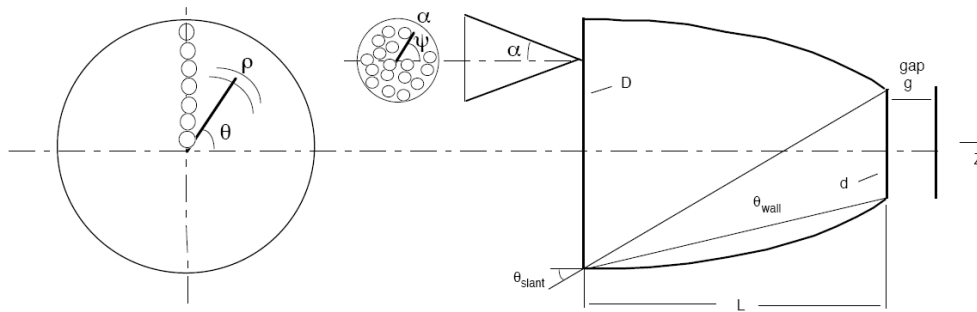


Fig. 4. Spatial and angular coordinates to be considered in the calculation of efficiency and concentration factor.

It is worth noting that the calculation fully includes skew rays. If the routine is limited to meridian rays, a serious error in η and C results, especially for large input NA_i .

Before presenting the results, the differences with previous works will be commented upon. In Refs [2,3], because of the interest in solar radiation applications, emphasis is on efficiency of collection rather than on concentration factor, and several interesting analytical results are derived for the 2-D case (meridian rays) or for asymptotic cases (either very small or large NA_i).

Other papers have considered miniaturized concentrators for diode-to-fiber coupling [4] and sophisticated geometries [5-7] for the solar concentration, yet without providing the performance of concentration factor versus NA. To our best knowledge, the asymptotic behaviour expressed by the straight lines in Fig.2 has not been reported before, and the application of non-imaging concentrator to array of detector is new as well. .

4. Results

Calculations have been performed for a range of input/output diameters of interest for the application to an intended SPAD (Single Photon Avalanche Detector) array [8] of large dimensionality (initially 32x32 and then up to 128x128). Pixel size is 50 to 70 μm , and detector size 7 to 10 μm , so that the theoretical achievable concentration factor spans from 25 to 200 with a central value of 50-60. Aim of the specific application is to demonstrate an on-board concentration of at least 30.

Fig.5 and 6 report the (power) concentration factor versus input numerical aperture, attained by an ideally reflective, hollow geometry, TCC and PPC, respectively. As it can be seen, at equal length of the concentrators, the PPC outperforms the TCC, which is attractive because it is easier to fabricate. However, though it does not attain the ideal performance, the TCC yields respectable concentrations, up to about 50-60 for a long (400-500 μm) device. On the other hand, a PPC with the same geometry (length and input/output diameters) starts with higher concentrations at small NA_i , close to the geometrical area ratio, but then decreases faster and approaches the TCC performance when the NA^{-2} asymptote (Fig.2) is reached.

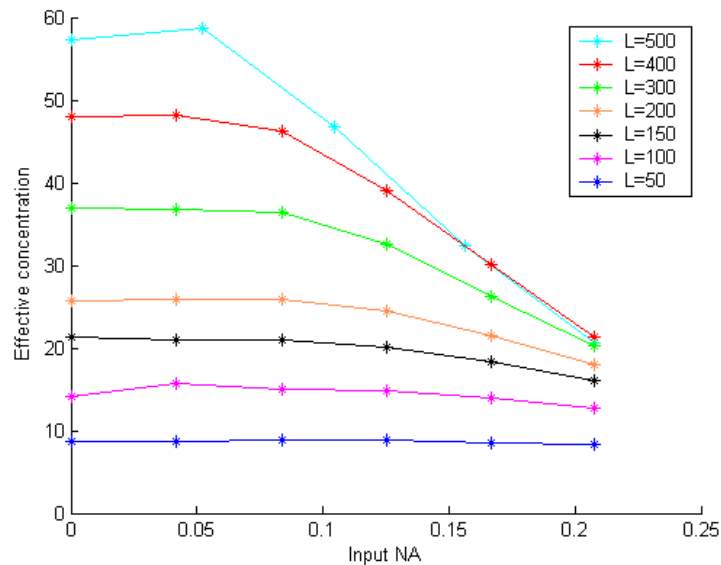


Fig. 5. Effective concentration C of the TCC versus the NA_i of input rays, filling a cone of rays up to NA_i , with length L as a parameter. Output diameter is 10 μm . Gap is $g=0$. Values of effective concentrations are, at small input angles, $C=65, 50, 40, 25, 21, 16, 11$, about 2-3 times less than the input/output area ratio of 200, 160, 120, 81, 61, 41, 20, and close to the $\sin^2 \alpha_{\text{wall}}$ values of 68, 55, 45, 25, 20, 15 and 10 (see Fig.3 for α_{wall}).

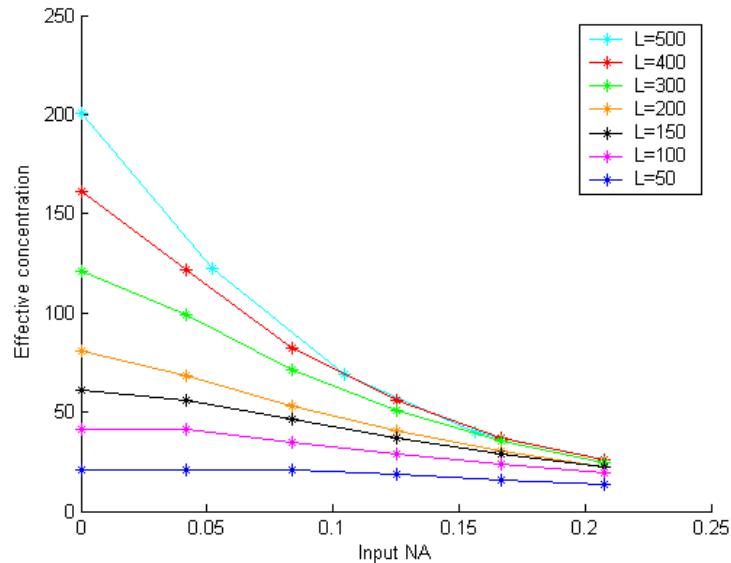


Fig. 6. Effective concentration of the PPC versus the NA_i of input rays, with length L as a parameter. Output diameter is $10\ \mu\text{m}$. Gap is $g=0$. To ease the comparison, input/output diameters are the same as for the TCC of Fig.5. Input diameters are: 142, 127, 110, 90, 78, 64, $46\ \mu\text{m}$. Values of concentration are consistently larger than those of the TCC and approach the geometrical area ratio at small NA, despite the fast roll off at high C.

The PPC is more difficult to fabricate, but a successful example based on 3-D diffuser lithography has been recently reported [9].

About the (reflective) CPC, the diagrams of concentration factor versus input NA for several values of concentrator length (126 to $1073\ \mu\text{m}$), corresponding to small-NA concentrations of 25 to 200, are reported in Fig.7. The four diagrams are for some values of gap, namely $g=0, 1, 2$ and $4\ \mu\text{m}$. As it can be seen, a gap up to about 20% of output diameter can be tolerated in a reflective CPC with a minor loss in concentration and allowed NA.

Several additional cases have been computed further, omitted here for conciseness. Detailed calculations have been carried out also for refractive concentrators, that is, geometries of TCC, PPC and CPC filled with a material with an index of refraction n , and with no other reflective feature. An interesting result is that, in practical cases (at least for $n=1.5$) filling the concentrator doesn't change appreciably the collection efficiency, because rays that are incident at low angle respect to the surface perpendicular (and miss total internal reflection) would be lost anyway (reflected back toward the entrance) if the structure has reflecting walls. On the other hand, a loss is incurred at the output interface if a gap is allowed there, because skew rays are subject total internal reflection instead of being refracted to the detector. We then assume either $g=0$ or a gap filled with the same index of refraction of the concentrator. In conclusion, for $g=0$, the refractive concentrator has nearly the same C vs. NA_i curve as the reflective concentrator when we rescale by n the numerical aperture of input rays. Another result summarizing the performance of concentrators is shown in Fig.8, where we plot concentration versus NA of reflective and refractive CPC, PPC and TCC.

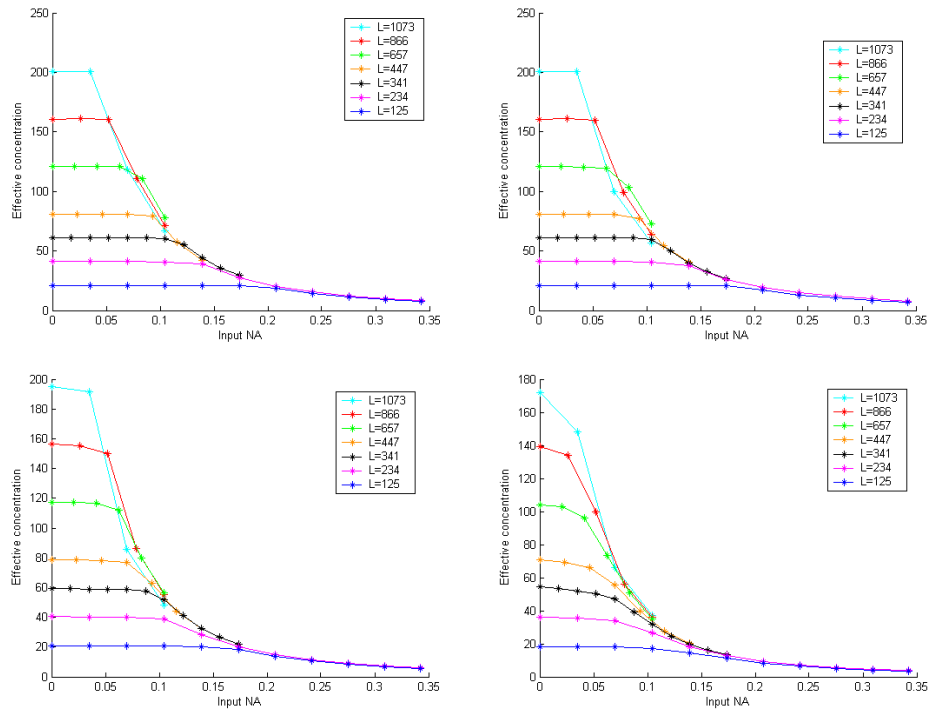


Fig. 7. Effective concentration of CPC versus numerical aperture and with length as a parameter. Concentrations corresponding to L are 200, 165, 120, 80, 60, 40, 20. The output diameter is $10\ \mu\text{m}$. Output gap to detector (from top left- to bottom right) is 0, 1, 2 and $4\ \mu\text{m}$.

From the results, the r-CPC has clearly the best performance, as it supplies a nearly constant concentration ($C=60$) up to about $\text{NA} = 0.2$ (or $f_{\#}=2.5$). However, if the specification is relaxed to say, $C=40$, also r-PPC and r-TCC can be used, with the advantage of a simplified construction.

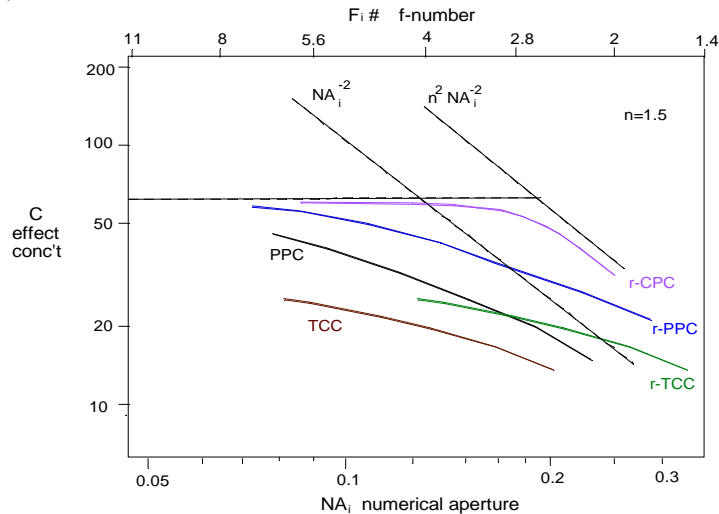


Fig. 8. Performance of TCC, PPC and CPC. reflective (no prefix) and refractive (r- prefix). Effective concentration is plotted vs input ray NA_i , and for a $g=1\text{-}\mu\text{m}$ air gap for reflective types. The concentrator length L is $150\ \mu\text{m}$ for TCC and PPC, and $350\ \mu\text{m}$ for the CPC. All have a geometrical area ratio concentration of 60.

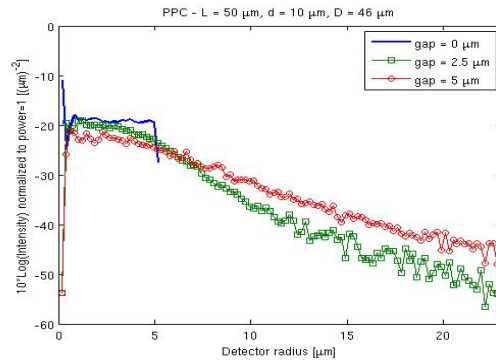


Fig. 9. Relative irradiance leaking out of a pixel of diameter $D=10\ \mu\text{m}$ as a function of distance, for a reflective PPC of $C=21$. Parameter is gap g (5 and $10\ \mu\text{m}$).

Last, it may be interesting to evaluate the crosstalk between adjacent pixels. For a reflective PPC the result of calculation of leaky rays collected vs. distance d is shown in Fig.9. Respect to radiance internal to the concentrator output, the diagram shows that at an off-axis of $25\ \mu\text{m}$ the irradiance is dropped of about 30 dB, a satisfactory figure.

5. Conclusions

We have demonstrated that non-imaging concentrators can supply a sizeable factor of recovery of the fill factor, trading solid-angle (input NA) for surface. We have calculated the concentration factors of three types of geometries, both reflective and refractive, and evaluated quantitatively the improvement achieved as a function of the input NA.

Acknowledgements

The authors wishes to thank Francesco Ingarozza for performing numerical calculations. This work has been supported by the European Community within the Sixth Framework Programme IST FET Open MEGAFRAME [“Million Frame Per Second, Time-Correlated Single Photon Camera”] project (contract No. 029217-2).

Disclaimer: This publication reflects only the author's (authors') views. The European Community is not liable for any use that may be made of the information contained herein.

Blank page